Carbon Capture Science & Technology 10 (2024) 100151

Contents lists available at ScienceDirect

Carbon Capture Science & Technology

journal homepage: www.elsevier.com/locate/ccst

Full Length Article

Chemical activation of porous carbon extracted from *biomass* combustion bottom ash for CO_2 adsorption

Mikhail Gorbounov[a], Emilie Diaz-Vasseur[a], David Danaci[b], Salman Masoudi Soltani[a,*]

[a] Department of Chemical Engineering, Brunel University London, Uxbridge UB8 3PH, UK
[b] Department of Chemical Engineering, Imperial College London, South Kensington, London, SW7 2AZ, UK

ARTICLE INFO

Keywords:
Carbon capture
Adsorption
Biomass combustion ash
Activated carbon
Chemical activation

ABSTRACT

Adsorption of CO_2 by solid sorbents has been proposed as a pathway to decrease the emissions associated with combustion of fuels. However, if employing the waste residues of the combustion process (e.g. biomass combustion bottom ash), a pathway towards a green circular zero-waste and zero-emissions economy may be achieved. As such, a carbonaceous adsorbent has been produced (*via* chemical activation) using biomass combustion bottom ash as a precursor. This process entailed an intelligently designed experimental campaign based on a randomised Taguchi L9 orthogonal array, which revealed moderate activation temperatures (~625 °C) and times (30 min) coupled with high ramp rates (10 – 15 °C/min) to be preferable. Following this method, a highly microporous (~93 %) material was produced possessing a surface area of 643.6 m^2/g. This, in turn, facilitated a substantial increase in CO_2 uptake, namely, 1.29 mmol/g at 50 °C (quadruple that of the parent carbon and double that of the physically activated counterpart). Additionally, the working capacity as well as the heat of adsorption were measured. The latter properties are often overlooked with main focus drawn towards purely the adsorption capacity; however, they are imperative for industrial deployment of CO_2 adsorbents.

1. Introduction

Climate change and its impact across the world is an ever growing and pressing concern that has been garnering increasing attention. Greenhouse gas (GHG) emissions, more specifically CO_2 emissions, play a significant role in climate change, being responsible for 80 % of the total amount of released GHGs in 2021 in the UK (Office for National Statistics, 2023). For the foreseeable future, even with the progression of green technologies (e.g. solar/wind energy), CO_2-heavy energy sources would still be a major part of the energy supply across the globe. Therefore, carbon capture and storage (CCS) technologies are expected to be vital to combat some of the associated CO_2 emissions in power, manufacturing and chemical sectors. This can be achieved by deploying particular point-source capture techniques followed by underground storage, thus preventing release of carbon dioxide into the atmosphere.

The energy sector is gradually developing more environmentally-conscious processes, aiming to slow down and/or reverse their contribution to global warming. For example, the biggest renewable power station in the UK (BBC, 2022), operated by Drax Group in Selby, North Yorkshire, aims to become carbon negative by 2030 (Drax, 2019), and has abandoned coal in favour of pelletised biomass. However, energy generation *via* combustion of biomass is accompanied by the generation of waste solid residues: fly ash (FA) and bottom ash (BA). This leads to ~170 MT of biomass ash per year across the globe (Zhai et al., 2021) highlighting the importance of managing this novel waste stream. Coal ashes find secondary applications (e.g. asphalt (Woszuk et al., 2019) and cement (Yun et al., 2022) filler manufacturing) yet their biomass combustion counterparts cannot be used in the same applications (Gorbounov, et al., 2023) due to excessive variation in biomass ash (Michalik and Wilczynska-Michalik, 2012) coupled with a greater content of alkaline/alkali-earth metals (e.g. Na, Mg, Ca) than those of coal ashes (Vassilev et al., 2010). These wastes have found alternative applications in the synthesis of zeolites from FA (Petrovic et al., 2021, 2022) and carbonaceous adsorbents from BA (Gorbounov et al., 2022). The latter option has been selected due to presence of a high amounts of unburnt biomass and carbon as part of BA. Utilising these combustion by-products would facilitate management of hazardous waste and waste valorisation as it would prevent the material from being directly landfilled, allowing biomass power generation companies to save on associated costs (standard and lowered rates in the UK as of 01.01.2023 are £102.10 and £3.25 per tonne, respectively).Furthermore, use of FA and BA as the precursor for capture media could decrease the system's carbon footprint by producing and deploying these sorbents for CO_2 adsorption on site, thus aligning with the UK's ambitions to be carbon-neutral by 2050 (BEIS, 2021) and minimise biomass waste ('UK Biomass Policy Statement', 2021).

* Corresponding author.
E-mail address: Salman.MasoudiSoltani@brunel.ac.uk (S. Masoudi Soltani).

https://doi.org/10.1016/j.ccst.2023.100151
Received 13 September 2023; Received in revised form 10 October 2023; Accepted 13 October 2023

Within that, the carbon derived from BA is an especially promising material. Classically, carbonaceous adsorbents can be produced from a large variety of sources, often from agricultural sector waste like rice husk (Nandi et al., 2023), garlic peel (Huang et al., 2019), sugar beet molasses (Kiełbasa et al., 2022), pine saw dust (Quan et al., 2020), bamboo (Ji et al., 2022) other woody materials and agro-waste (Bade et al., 2022; Ketabchi et al., 2023). However, prior to application as sorbents, the materials have to be treated using methods such as chemical activation or physical activation. These methods aim to increase the surface area and pore volume of the carbonaceous materials, producing/opening nanopores that would be beneficial for CO_2 adsorption.

Key differences between these activation methods include the energy requirements, activating agents used and synthesis times, amongst a plethora of other factors that may differ depending on the precursor, activation conditions and activating agents. Typically, physical activation uses high temperatures and oxidising gases (e.g. CO_2 and/or steam), whilst chemical activation involves impregnation of the carbonaceous precursor by a chemical activating agent and a washing step after activation (Ketabchi et al., 2023). There are a number of different activating agents employed in chemical activation; however, acids (e.g. H_3PO_4, H_2SO_4), salts (e.g. $FeCl_3$, $ZnCl_2$) and bases (e.g. KOH, NaOH) have been most-commonly reported in the literature (Taylor and Masoudi Soltani, 2023).

Naturally, there are benefits and limitations to physical and chemical activation methods (as well as to different activating agents for the latter). However, with regards to porosity generation, the benefits of chemical activation often outweigh its limitations. Specifically, potassium hydroxide (KOH) is known for effective development of microporosity; therefore, this material is often opted for as the activating agent in the context of CO_2 adsorption (Wang et al., 2022; Quan et al., 2023). On the other hand, KOH is not only corrosive but also environmentally dangerous and can lead to reaction equipment destruction (Bai et al., 2023).

The activation mechanism is mainly based upon two overlapping redox reactions (Taylor and Masoudi Soltani, 2023):

$$6KOH + 2C \rightarrow 2K + 2K_2CO_3 + 3H_2 \uparrow$$

$$4KOH + C \rightarrow 4K + CO_2 \uparrow + 2H_2O \uparrow$$

However, a multiplicity of other reactions involving KOH, the evolved gas molecules and other by-products are also believed to occur further contributing to porosity development (Heidarinejad et al., 2020; Nandi et al., 2023).

$$2KOH \rightarrow K_2O + H_2O \uparrow$$

$$K_2CO_3 + 2C \rightarrow 2K + 3CO \uparrow$$

$$2K_2CO_3 + C \rightarrow 4K + 3CO_2 \uparrow$$

$$K_2O + C \rightarrow 2K + CO \uparrow$$

$$C + CO_2 \rightarrow 2CO \uparrow$$

$$C + H_2O \rightarrow CO \uparrow + H_2 \uparrow$$

$$K_2O + C \rightarrow K + C - O - K$$

Upon activation the activated carbon (AC) has to be washed to remove residual metallic species. Although, some potassium may intercalate into the carbon structure in-between the carbon layers or remain as part of the sorbent in form of quasi-chemically bound potassium-oxygen functionalities (Liu et al., 2015). However, the exact activation conditions resulting in most suitable textural properties and surface morphology vary significantly across the plethora of potential precursors and applications. As such, identification of the most suitable operating envelope is highly important for optimisation of the activation process. This can be achieved by deploying an intelligent design of experiments (DoE) framework followed by analysis of variance (ANOVA) and response surface methodology (RSM) (Gorbounov et al., 2022). These allow to evaluate the experimental results, identify the impacts of individual parameters as well as any interactions amongst them and the residual error in order to produce a polynomial equation that facilitates maximising of the chosen dependant variable (Karimi et al., 2023). Unfortunately, this aspect of the activation process has largely been overlooked within the current literature, and therefore, its implementation is not only timely, but also critical in complete optimisation of the process. Herein, we have produced and executed a randomised experimental campaign employing a Taguchi L9 orthogonal array in order to maximise the CO_2 adsorption capacity of the biomass combustion bottom ash-derived carbonaceous adsorbent.

2. Materials and methodology

2.1. Chemical activation of carbon

The parent biomass combustion bottom ash-based carbon was derived as per the procedure outlined in our previous works (Gorbounov et al., 2021; Gorbounov et al., 2023). KOH (85 % pure; CAS 1310-58-3; Alfa Aesar) was employed as the chemical activating agent. A randomised Taguchi L9 orthogonal array was applied to study the design space, with the evaluated factors being the activation time (τ_{act}) and temperature (T_{act}), ramping rate (RR) as well as the impregnation ratio (IR) of the virgin carbon to KOH.

To start, an appropriate amount (as per the randomised experimental campaign matrix) of the materials was weighed before being transferred to a pestle and mortar, where the potassium hydroxide was manually crushed and mixed with the carbon (i.e. dry mixing). The mixture was then transferred into an activation vessel (i.e. ceramic boat) and placed into the centre of an insulated Inconel tube located in the furnace (Carbolite Gero TF1 12) under 300 mL/min of N_2 (BOC, purity of N4.8). Upon completion of the thermo-chemical treatment, the samples were washed with deionised (DI) water using a Büchner flask-funnel system until the pH of the filtrate reached 7 (approximately). The resulting material was then analysed as per Section 2.2. The optimisation of the synthesis procedure was focused on maximising the CO_2 adsorption capacity and was carried out using Response Surface Methodology (RSM) as well as *via* studying the corresponding Signal-to-Noise (S/N) ratio. The statistical analysis (as well as the development of the experimental matrix) was conducted in Minitab (version 18).

2.2. Adsorbent characterisation

The CO_2 uptake of the produced adsorbents was evaluated *via* thermogravimetric analysis – TGA (Mettler Toledo TGA 2) using high purity gases, i.e. N_2 (N 4.8) and CO_2 (N 2.8), purchased from BOC. The programme commenced with a 15 min purge at 150 °C using 50 mL/min of nitrogen to eliminate pre-adsorbed matter. Afterwards, the sample was cooled (−10 °C/min) to the desired adsorption temperature where the gas was switched to pure carbon dioxide for a 30 min adsorption step. Proximate Analysis was also conducted in the TGA as per (ASTM, 2013). Further, Fourier Transform Infrared Spectroscopy (Shimadzu IRSpirit) as well as Scanning Electron Microscopy/Energy Dispersive X-ray Spectroscopy (JOEL IT200) were employed to characterise the sorbent. The latter was conducted using a copper plate as background material. The porosity was evaluated by obtaining the Brunauer – Emmett –Teller surface area (S_{BET}) as per (Brunauer et al., 1938) on a Micromeretics ASAP 2020 sorption analyser, using N_2 at 77 K. Prior to which, the material was purged (i.e. degassed under N_2) at 200 °C (ramping rate of 5 °C/min) for 6 h.

The Fourier Transform Infrared (FTIR) spectra were obtained by employing the standard Attenuated Total Reflection (ATR) method to minimise the use of KBr, in the region of 4000 and 600 cm^{-1} (20 scans

at a resolution of 4 cm^{-1}). The Scanning Electron Microscopy/Energy Dispersive X-ray Spectroscopy (SEM/EDS) was conducted using copper plates (to prevent confusion of the sample elements and background). Additionally, the samples were not gold-coated as the carbonaceous nature of the samples facilitated electrical conductivity.

Elemental Analysis was conducted using acetanilide as a standard material *via* a Flash 2000 Organic Elemental analyser (Thermo Scientific).

The heat of adsorption was calculated based on the volumetric CO_2 adsorption isotherm measurements at 0, 10, 20, 30 and 40 °C. Prior to the experiments, the material was degassed *ex-situ* at 350 °C overnight at a vacuum level of 0.1 $mbar_a$. The temperature was increased stepwise to 50, 100, 200, and finally 350 °C when the vacuum level reduced back to 0.1 $mbar_a$. The isotherms were measured on a 3Flex (Micromeritics Instruments Corporation), and *in-situ* degassing was performed at 350 °C for two hours before each measurement. The isotherm data has also been provided as supplementary information in AIF format (Evans et al., 2021).

3. Results and discussions

3.1. Activation and optimisation campaigns

A randomised four-parameter (at three levels each) L9 Taguchi DoE framework was developed prior to commencement of the experimental campaign. The factors and their respective values (presented in Table 1) were based on an extensive literature review in conjunction with initial trials used to identify the appropriate design space.

The obtained results were evaluated *via* analysis of variance (ANOVA) with the dependant variable being the CO_2 adsorption capacity. The regression coefficient (R^2) of the produced model was calculated to be 0.9995. The predictive ability of the model, i.e. R^2_{pred}, was learned to be slightly weaker displaying a value of 0.9429. The latter parameter is of utter importance when dealing with a high value of the regression coefficient as it may stem from an overly complex model that is fitting random noise alongside the response signal(s). To determine R^2_{pred} every singular datapoint is removed from the set and the regression equation estimates each individual removed point, thus determining the predictive capabilities of the model. The results of the statistical analysis are presented in Table 2 and, as expected, some of the parameters had a paramount impact on the process, whereas other were found to be not statistically significant (NSS). This is based on the F- and p-values which are (in simplified terms) *the variation between the sample means versus the variation within the sample set (i.e. mean square between groups over mean square within groups)* and *the probability of observing such a F-value under the given null hypothesis*, respectively.

Table 1
Factors at the respective levels examined in the Taguchi L9 design.

Parameter	Levels		
Activation Time (τ_{act}), min	30	60	90
Activation Temperature (T_{act}), °C	400	625	850
Ramping Rate (RR), °C/min	5	10	15
C:KOH Impregnation Ratio (IR)	1:1	1:2	1:3

Table 2
Results of the ANOVA for the conducted experimental campaign.

Parameter	F-Value	p-Value	Significance
Activation Time (τ_{act})	25.67	0.124	NSS
Activation Temperature (T_{act})	241.31	0.041	3
Ramping Rate (RR)	470.01	0.029	2
C: KOH Impregnation Ratio (IR)	29.57	0.116	NSS
Quadratic Interaction of τ_{act}	162.18	0.050	4
Quadratic Interaction of T_{act}	1152.88	0.019	1
Quadratic Interaction of IR	43.69	0.096	NSS

The presence of non-linear relationships within the design space is evident based on the data presented in Table 2, with the quadratic term of T_{act} being the most statistically significant (followed by the impacts of RR (linear), T_{act} (linear) and $\tau_{act}{}^2$). Similar observations can be made when evaluating the S/N ratios shown in Fig. 1a. S/N ratio is a measure of robustness of the process that assesses how resistant a process is to the changes in the input parameters. Since the goal of the experimental campaign was to maximise the adsorption capacity of the produced AC, the "larger is better" approach (Eq. (1)) was chosen for the analysis of the S/N ratios.

$$\frac{S}{N} = -10 \cdot \log\left(\sum\left(\frac{1}{y^2}\right)/n\right) \tag{1}$$

In Eq. (1) y stands for the given response stemming from the parameter-level combination and n is the number of responses of that parameter-level combination.

Based on the gathered data alongside the conducted analysis, activation temperature and time as well as the RR are found to significantly influence the adsorption capacity of the produced sorbent. The quadratic effect of T_{act} is also evident from Fig. 1; which is associated with activation at excessively high temperatures resulting in micropores collapsing and producing mesopores instead (which are less desirable than micropores in the context of CO_2 adsorption). On the other hand, i.e. low temperatures, chemical activation has not reached its "full potential" as signalled by the higher S/N ratios. Moreover, the RR plot presents a linear increase, suggesting longer thermo-chemical treatment times to be

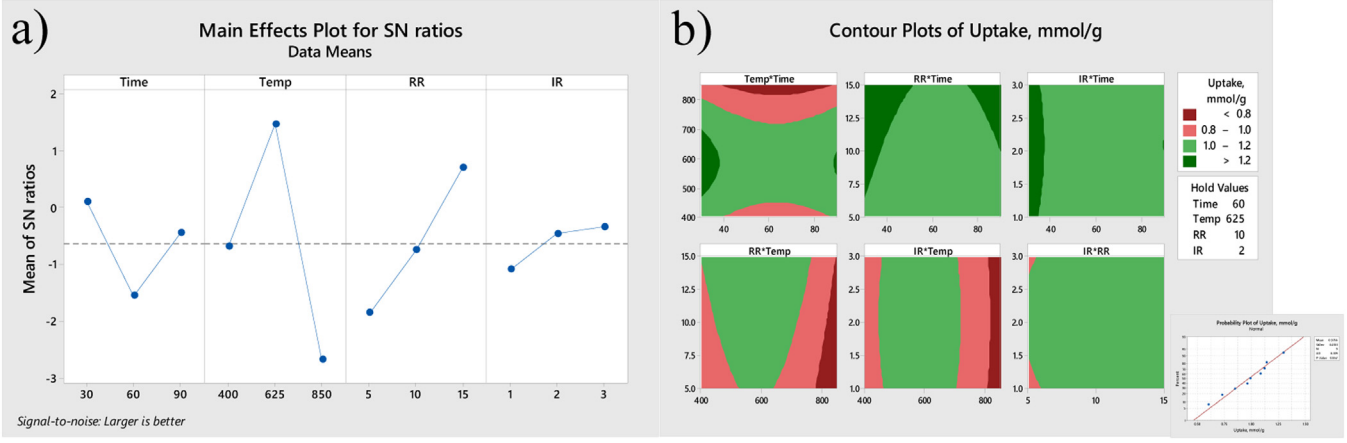

Fig. 1. (a) the S/N ratio for the evaluated L9 array (lines are to guide the eye only) and (b) contour plots of CO_2 uptake with the normality plot on the bottom right.

less desirable in terms of CO_2 adsorption capacity (as well as product yield). Therefore, larger RRs were found to be beneficial (in terms of both attractiveness of sorbent and cost of material production). Interestingly, the impregnation ratio was found to be NSS. However, similar conclusions (i.e. change of the C:KOH ratio does not drastically impact the CO_2 adsorption capacity at 50 °C) could be made if evaluating data available in the literature (Nandi et al., 2023). Nevertheless, this phenomenon, could be attributed to the inherent heterogeneity of the dry mixing process. As such, future works might endeavour to avoid using this technique and opt for wet mixing. However, this would, in turn, lead to an alternative issue. The aqueous KOH solution would etch away at the (ceramic) crucible/boat instead of activating (to the "full potential") the carbonaceous sorbent resulting in an additional variation source and/or lurking variable as well as activation vessel degradation. Further, the quantities of the main exchangeable cations may be reduced by activation with this alkaline solution (Sajjadi et al., 2019). In case of biomass combustion bottom ash-derived carbons, Ca^{2+} may be the main victim of this phenomenon. A decrease in such cations might result in a lower electrostatic potential of the adsorbent, hence, leading to reduced capture capacity *via* physical adsorption.

Further, as hinted at previously, both the fastest RR as well as the minimum τ_{act} are shown to be most beneficial across their evaluated levels. This combination may imply a potential for a reduction of energy requirement for this thermochemical AC synthesis route by further dropping the activation time and further enhancing the ramping rate. This hypothesis is corroborated by the contour plots (Fig. 1b) produced as part of the RSM.

When employing a Taguchi DoE, the optimal conditions are deduced based on the calculated S/N ratio. In this case (since the aim is to maximise the dependant variable), the suggested levels would be: 30 min, 625 °C, 15 °C/min and an IR of 1:3. On the other hand, RSM optimisation proposed a slightly different temperature and IR (595.5 °C and 1:2.23, respectively), whereas RR and τ_{act} were the same. However, neither of these experiments achieved the adsorption capacity predicted by the model. Such outputs might be associated with the uncontrollable variation inherent in waste or (as highlighted previously) the heterogeneity of dry mixing as well as a lower predictive capability of the model. Future research might, perhaps, employ a design with repeated runs (classically, at the centre points) to facilitate the incorporation of the inherent heterogeneity of dry mixing into the design space. Additionally, when dealing with a L9 array and analysing four factors at three levels each, the model is inherently overfit (i.e. less degrees of freedom than terms that are estimated). Therefore, such model can be reduced by eliminating terms (in this case the interactions as well as the quadratic effect of RR) to allow for statistical analysis. This limitation is unavoidable for such a design. Future research, therefore, may focus on optimisation of the production of such sorbent *via* a different DoE framework (e.g. Central Composite design, Box-Behnken design). Although these designs are more complex and involve a much more extensive/comprehensive experimental campaign, they would, in turn, allow for higher accuracy.

Nevertheless, the experimental campaign produced sorbents with a much higher CO_2 uptake with one of the samples outperforming the rest. The material that was chosen for further characterisation (labelled as ChAB) was obtained at the design point corresponding to 30 min of chemical activation at 625 °C with a ramping rate of 10 °C/min and an IR of 1:2. These conditions allowed for a final product mass yield of 36 %.

3.2. Scanning electron microscopy/energy dispersive X-ray spectroscopy

Scanning Electron Microscopy/Energy Dispersive X-ray Spectroscopy (SEM/EDS) are common analytical methods for exploring the surface morphology (Fig. 2) alongside the surface elemental composition of a given sample. Hence, their use in analysis of ChAB.

The morphology of ChAB is, as expected, a fine powder with a highly rough surface. This can be attributed to a combination of effects stemming from the parent virgin carbon as well as resulting from the process of chemical activation. A further impact of the latter can be noted when evaluating the surface elemental composition of ChAB.

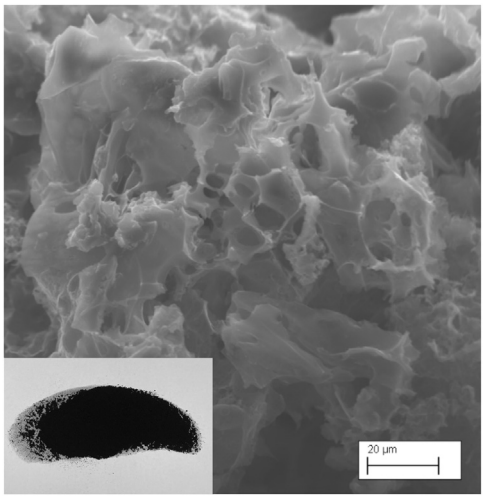

Fig. 2. SEM image of ChAB with full-scale photo as insert.

EDS analysis suggests some residual presence of potassium (1.6 %) which has not been alleviated during the washing step post-activation. This phenomenon is associated with DI water mainly removing potassium carbonate (and/or potassium oxide) formed as by-product of activation (Liu et al., 2015). However, during activation K-containing species also diffuse into the internal structure of the carbon as part of pore creation and widening/opening (Sajjadi et al., 2019) and free potassium would penetrate between the graphene layers of the AC (Heidarinejad et al., 2020) These intercalated metal atoms are believed to occupy the position between the centres of the C hexagons of adjacent graphitic layers (Kaloni et al., 2012) and have been shown to increase AC's affinity towards CO_2 as well as surface polarity (Liu et al., 2015). The latter may occur as intercalation involves electron transfer from the metal to the delocalised π-electron cloud of the graphene sheets (Taylor and Masoudi Soltani, 2023). However, quantities of slightly over 1 % of K are believed to provide maximum benefit from intercalation (Liu et al., 2015), which is the case for ChAB as elemental potassium is scarce and sparse (1.6 wt%) in the analysed sample. Interestingly, no Si and/or Al have been picked up during the single-point measurements. This might be associated with the surface nature of EDS; hence, bulk analysis techniques would be better suited for holistically investigating ChAB and quantifying the inorganics. Alternatively, the aluminosilicate-based ash impurities may have been (partially) eliminated due to their reaction with KOH, producing water soluble salts that were carried away during the final washing stage of AC production. Further, EDS has intrinsic limitations when quantifying elements with a lesser atomic mass than that of sodium (due to lighter elements emitting weaker signals that may have been absorbed by the specimen before reaching the detector (Konopka, 2013)), hence, the estimations of C (70.2 %) and O (28.6 %) may be less accurate. As such, bulk analysis techniques are required to evaluate the composition of the produced sorbent.

3.3. Elemental analysis

One of such bulk analyses is elemental analysis (often also referred to as CHN(S)-analysis or *ultimate analysis*). It allows for estimation of the elemental C quantities readily (as opposed to EDS). The process involves combusting the sample in pure O_2 in order to quantify elemental C, H and N based on their final/full combustion products. The resulting gases are then separated (e.g. gas-phase chromatography) and measured (e.g. *via* thermal conductivity detectors).

The reduction in C content (39.34 %) compared to the parent material (Gorbounov et al., 2023) are to be expected due to the intrinsic effects of the activation process. Interestingly, no nitrogen was found in ChAB. This is, however, unsurprising as KOH activation is not known for producing nitrogen containing functional groups. Nevertheless, the decrease in the nitrogen (0.00 %) and hydrogen (2.05 %) contents (compared to the parent virgin carbon) might stem from the loss of volatile organic compounds (VOCs), which has been next quantified *via* proximate analysis.

3.4. Proximate analysis

An alternative bulk analysis method is *proximate analysis*. It allows to quantify, firstly, the moisture and VOC content by increasing the temperature under an inert gas flow to appropriate temperatures as per ASTM D3172 (ASTM, 2013). Afterwards the gas is switched to an oxidising atmosphere (pure oxygen or air) to allow for loss of fixed carbon. The amount of the latter is calculated based on the ash that has remained in the crucible at the end of the test.

As expected, upon chemical activation, the percentage of VOCs (20 %) has notably decreased compared to the parent material (Gorbounov et al., 2023). This is attributed to the activation being conducted at elevated temperatures, leading to the evolution of VOCs off the surface of the adsorbent. This decrease may, in turn, have inflated (in percentage terms) the amount of ash (to 33.5 %). However, this also may stem from their lesser dissolution due to dry mixing as well as some additional potassium-based inorganic components. Furthermore, the fixed carbon content (33 %) is in agreement with the data gathered *via* ultimate analysis. Lastly, the increased amount of moisture (13.5 %) retained by the sample may be attributed to the elevated surface area as well as the presence of surface functional groups that can be visualised from spectroscopic analysis. These techniques can also elucidate the nature of the ash impurities.

3.5. Spectroscopic analysis

The presence of the silica-based ash impurities has been further corroborated *via* Fourier Transform Infrared Spectroscopy (FTIR). Additionally, the produced spectrum for the ChAB sample shows a number of different identifiable peaks (Fig. 3).

Starting from left to right, the first band is located at ~ 830 cm^{-1} and can be accredited to the bending vibrations of the C–H bonds found in the sample (Merck, 2023). The next identifiable peak is found at ~957 cm^{-1} and corresponds to the vibrations of Si–O bonds that are characteristic of ash particulates (Assad Munawar et al., 2021). This is to be expected as the AC is derived from biomass combustion ash, hence, the presence of some impurities of this nature. Further, the C–O functionalities have been identified at ~1306 cm^{-1} and also at ~2100 cm^{-1} (Williams et al., 2022; Merck, 2023). These peaks may also stem from the quasi-chemical bonds that allow the potassium to remain (after

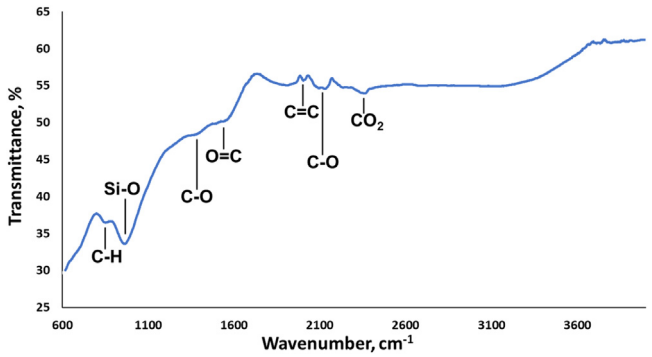

Fig. 3. FTIR spectrum of ChAB.

washing with deionised water) as part of the adsorbent in form of a C–O–K functionality (Liu et al., 2015). Additionally, peaks representing O=C and C=C at 1530 cm^{-1} and 1992 cm^{-1}, respectively, were identified. The former may stem from keto- or quinone-like structures (Shafeeyan et al., 2010), while the latter was ascribed to the asymmetric stretching of C=C bonds (*Map: Organic Chemistry (Wade), Infrared Spectra of Some Common Functional Groups*, 2020). Finally, the peak found at ~2358 cm^{-1} can be attributed to background CO_2 (Derrick et al., 1999).

The identified peaks are largely in-line with the typical FTIR peaks for KOH-activated carbons (Sajjadi et al., 2019); however, degradation of some surface functional groups in the presence of KOH has also been suggested in the literature (Nandi et al., 2023). Further, thermal treatment also promotes loss of volatiles, hence, some functionalities. As such, the presence or lack of functional groups can have a pronounced effect on the adsorption capacity of the material, for instance, by acting as active adsorption sites (classically, in the cases of chemisorption) or by producing a distribution of electrical charge on the surface of the carbon (impacting physisorptive properties). However, apart from the aforementioned factors, the porous structure and surface area play a key role in determining the uptake capacity. This is discussed in the following section.

3.6. Porosity and surface area analysis

The BET analysis is a common method for evaluation of the surface area for a given sorbent. In the case of ChAB, the S_{BET} has been calculated using the P/P_0 region of 0.13 and 0.32 to be 643.6 m^2/g (comparing to the parent carbon with 4.6 m^2/g and the physically-activated analogue with 248 m^2/g (Gorbounov et al., 2023)) with the N_2 adsorption isotherm obtained at 77 K (shown below in Fig. 4). As an alternative, the BET surface area was also determined based on the CO_2 isotherms at 0 °C. For this, the calculations were performed using SESAMI with default settings (Sinha et al., 2019; Terrones et al., 2023), an adsorbed cross-sectional area of 21.8 $Å^2$ (McClellan and Harnsberger, 1967) and a saturation pressure of 34.851408 bar_a (Lemmon et al., 2023). The latter method suggested the results to be slightly higher, namely, 687 m^2/g.

As evident from Fig. 4, ChAB presents a type IV physisorption isotherm featuring a type H4 hysteresis. Such loops are common when dealing with carbonaceous adsorbents (especially if significant burn off upon activation is observed (Bottani and Tascón, 2008)) which possess slit-shaped micropores (Rouquerol et al., 2013). This hypothesis of KOH activation leading to highly microporous powdered ACs (Molina-Sabio and Rodríguez-Reinoso, 2004) is further corroborated by ChAB's t-plot microporous area of 597.9 m2/g, hence, constituting ~93 % of the total surface area. However, an observed hysteresis loop in general suggests presence of pore sizes of over 4 nm (Thommes et al., 2015) also to be present on the surface of the AC. These observations are confirmed by pore size distribution plot (as seen insert of Fig. 4) and the average pore size of 4 nm (summarised in *Table 3*).

As such, the proposed activation conditions lead to a mesoporous material with a significant degree of microporosity. The latter is believed to be most beneficial for increasing CO_2 adsorption by providing a substantial portion of the pore volume and surface area thus to a considerable extent determine the uptake of an AC (Bansal and Goyal, 2005) as well as by increasing the material's affinity towards the gaseous adsorbate (Patel et al., 2017; Petrovic et al., 2022); whereas the former assist with diffusion of CO_2 into the framework, hence enhancing the overall adsorption kinetics. These phenomena can be corroborated by the conducted investigations in Section 3.7.

3.7. CO_2 adsorption studies

Most experiments reported in the literature on the topic of CO_2 adsorption in the post-combustion CCS context, have been run at an adsorption temperature of 25 °C. However, industrial flue gas discharged from the stack is more often received in the temperature range of 40 –

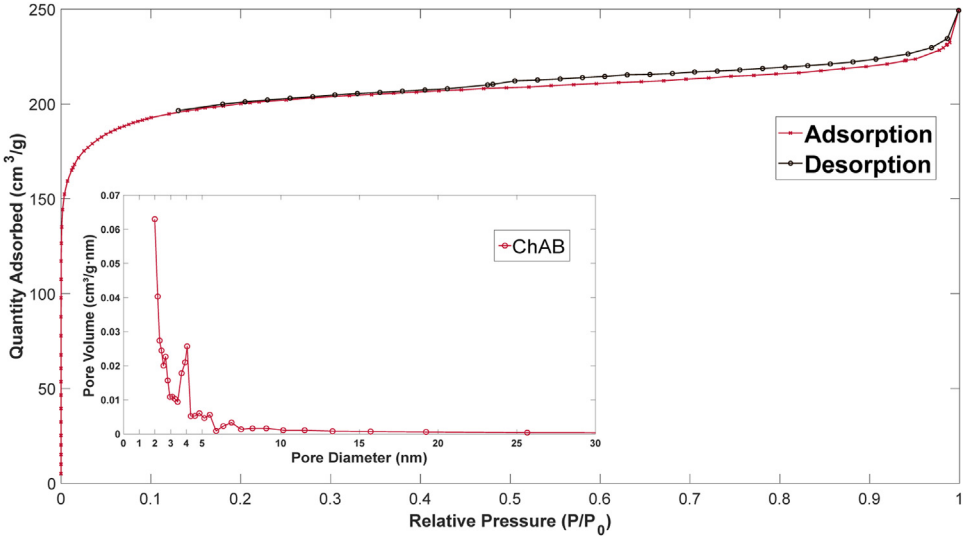

Fig. 4. BET N_2 adsorption isotherm of ChAB with the pore size distribution plot as insert (lines are to guide the eye only).

Table 3
Textural properties of ChAB based on the BET N_2 adsorption isotherm.

BET surface area, m^2/g	Micropore area, m^2/g	Micropore volume, cm^3/g	Average pore size, nm
643.6	597.9	0.29	4.0

Table 4
Comparison of CO_2 uptakes of ChAB and other samples (1 bar at 25 °C).

Sample	Activation technique	Uptake, mmol/g	Reference
Biomass combustion bottom ash-derived AC	Chemical (KOH)	1.93	(This work)
Biomass combustion bottom ash-derived AC	Physical (CO_2)	1.04	(Gorbounov et al., 2023)
Commercial AC	Physical	1.23	(Gorbounov et al., 2023)
Commercial AC	Physical (steam)	1.88	(Rashidi and Yusup, 2021)
AC from petroleum coke	Chemical (K_2CO_3)	2.26	(Rashidi and Yusup, 2021)
N/S doped AC from chestnut shell	Chemical (KOH)	3.16 – 4.54	(Ma et al., 2022)
N doped AC from macadamia nut shell	Chemical (KOH)	3.76 – 4.35	(Bai et al., 2023)
AC from coconut shell	Chemical (KOH)	3.16 – 4.15	(Bai et al., 2023)

80 °C. As such, uptake at these relevant temperatures is believed to be a more appropriate metric. On this ground, the adsorption capacity (at 1 bar) at not only 25 °C but also 50 °C and 75 °C were calculated to be 1.93 mmol/g, 1.29 mmol/g and 0.84 mmol/g, respectively.

The chemical activation with KOH facilitated a substantial increase in the uptake compared to the virgin carbon powder (Gorbounov et al., 2023). At 25 °C and 50 °C the uptake is approximately quadruple that of the parent material, whereas at 75 °C ChAB adsorbed six times more CO_2. Further, the uptake of ChAB at 50 °C is double that of the physically activated biomass combustion bottom ash-derived AC (Gorbounov et al., 2023). Apart from ChAB's physically activated analogue, the material has also been compared to other alternative sorbents (Table 4).

However, apart from these values, investigations into the applicable equilibrium adsorption isotherms (Section 3.7.1) are paramount to envisage the capacity and behaviour at more appropriate to post-combustion CCS concentrations of carbon dioxide. Additionally, kinetic (Section 3.7.2) and cyclic (Section 3.7.3) adsorption studies as well as heat of adsorption data (Section 3.7.4) are often overlooked despite being paramount for industrial deployment.

3.7.1. Equilibrium adsorption studies

Equilibrium isotherm models are a pivotal point in understanding of both the mechanism of adsorption as well as characterising the adsorbent-adsorbate interactions, the adsorbent surface and etc. (Hossain et al., 2013; Calzaferri et al., 2022; Zhang et al., 2022). Classically, Freundlich and Langmuir models are commonly applied to the data (Masoudi Soltani et al., 2015). Additionally, the Toth isotherm can also often be used to describe adsorption from gaseous media as

Table 5
Equilibrium isotherm models employed in this work.

Equilibrium isotherm name	Equilibrium isotherm equation
Freundlich	$q_e = K_F \cdot P^{1/n}$
Langmuir	$q_e = \frac{q_{max} \cdot K_L \cdot P}{1+K_L \cdot P}$
Multi-site Langmuir	$q_e = \sum_{i=1}^{z} \frac{q_{max(i)} \cdot K_{L(i)} \cdot P}{1+K_{L(i)} \cdot P}$
Toth	$q_e = \frac{q_{max} \cdot K_T \cdot P}{\left(1+(K_T \cdot P)^n\right)^{1/n}}$

it avoids some challenging aspects of the previously mentioned fundamental models (Mozaffari Majd et al., 2022). An alternative approach to overcoming some of their limitations is to apply the Multi-site Langmuir adsorption isotherms. As such, herein, these isotherm models have been applied to the CO_2 adsorption data of ChAB: (in alphabetical order), Freundlich, Langmuir, Multi-site Langmuir (namely, Dual-site and Tri-site Langmuir) and Toth isotherms as presented in Table 5.

The goodness-of-fit of the models has been evaluated non-linearly using the regression coefficient, R^2, and the normalised root mean square error (NRMSE) following our previous work (Gorbounov et al., 2023). Adopting non-linear regression instead of linear regression (the more commonly-employed method in the literature) allows for more accurate description of the system. The results of such fitting are shown in Fig. 5.

The Triple-site Langmuir isotherm is believed to provide the most accurate fitting to this chemically activated carbon, suggesting ChAB to possess a heterogenous surface with different types of active sites to

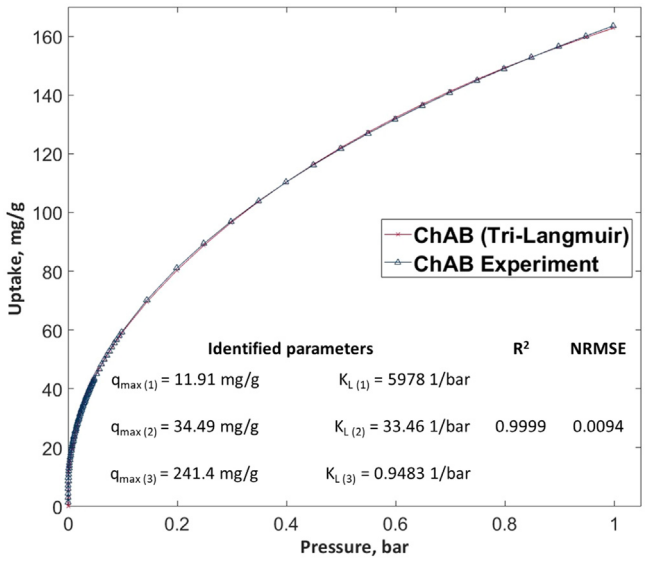

Fig. 5. Comparison of equilibrium adsorption model and experimental data at 0 °C as well as the parameters of the best fit and the results of the error analysis.

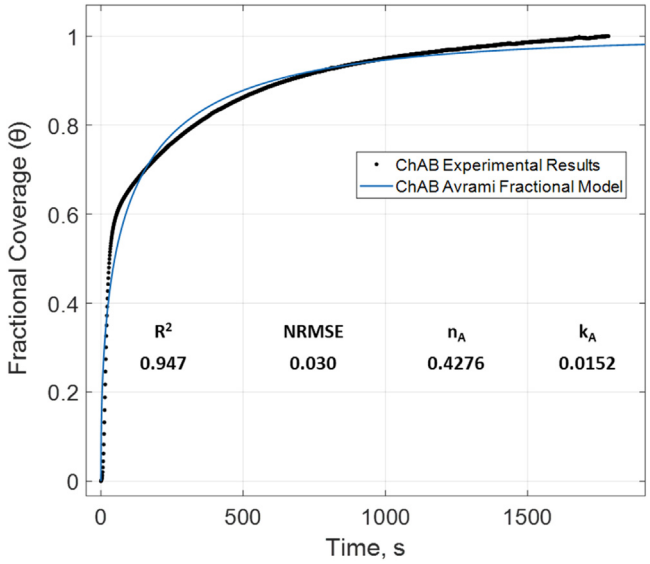

Fig. 6. Kinetics of CO_2 adsorption on ChAB at 50 °C.

be present as well as, possibly, involving different adsorption mechanisms. These might stem from different surface functional groups, presence of both crystalline and amorphous carbon as part of the AC structure or varying pore sizes (i.e. micro- and mesopores which would undergo volumetric filling and capillary condensation, respectively). In volumetric filling, the (in this case) CO_2 molecule occupies the pore "fully" due to the similar size of the adsorbate and the pore radius (Dubinin, 1975). This phenomenon is dependent upon overlap of adsorption force fields/potentials of the pore walls (Bottani and Tascón, 2008) and does not involve phase-change of adsorbate. Meanwhile, capillary condensation occurs when the CO_2 molecules undergo multilayer adsorption producing a condensed adsorbed film on either side of the mesopore wall, which would then bridge the gap between them forming a meniscus (Hattori et al., 2013). This phenomenon is ascribed to the saturation vapour pressure for the confined adsorbate phase to be higher than the condensation pressure due to surface tension effects and a reduction in free energy of the adsorbate in the pore(Bansal and Goyal, 2005).

3.7.2. Kinetic studies

In addition to the equilibrium capacity, an understanding of the adsorption kinetics is also imperative, especially when considering the inherently dynamic nature of CO_2 adsorption processes. In addition, key insight into the adsorption process can be deduced *via* adsorption kinetic models such as: Pseudo-First Order (PFO), Pseudo-Second Order (PSO), Modified Ritchie, Avrami, Elovich and Intraparticle Diffusion. As such, ChAB adsorption data has been non-linearly fit to the equations presented below.

As with the equilibrium isotherms, the fitness of the models from Table 6 has also been evaluated using the R^2 and the NRMSE. Additionally, partially based on recommendations by Simonin (2016), the models have also been evaluated using their fractional form. Regardless of the approach, however, the equations presented highly similar results and followed the same trends, namely, Avrami, Elovich, Modified Ritchie, PSO, Intraparticle Diffusion, PFO (in descending order). As such, the Avrami equation is believed to provide the best description for the process, although its applicability towards adsorbate-adsorbate systems has faced some criticism (Oladoja, 2016). The calculated fitting parameters are summarised in Fig. 6.

The calculations suggest n_A to be fractional. In such cases, the Avrami model is believed to be complex and multi-pathway (Songolzadeh et al., 2015), potentially following different kinetic orders and/or changing whilst the adsorbent-adsorbate system is in contact (Sivarajasekar and Baskar, 2019). This phenomenon would be in line with the best fit of the Dual-site Langmuir equilibrium model.

3.7.3. Cyclic adsorption studies & adsorbent's working capacity

The cyclic adsorption capacity is much more seldomly evaluated in the literature in stark contrast to industrial needs and requirements for wide adoption of CCS. Herein, the ChAB sample's cyclic working capacity was evaluated *via* a temperature swing process. The adsorption temperature was kept at 50 °C, whereas the initial purge as well as the desorption temperatures were held at 150 °C. Furthermore, the gas supply was switched from 50 mL/min of pure CO_2 to 50 mL/min of pure N_2, respectively.

The decrease in uptake can be seen from Fig. 7. The sharp drop of 4% from the first cycle to the second is a clear indication of the importance of such evaluations. Further, the rate of decline slows down leading to a 2 % decrease between cycles 2 and 3. After 10 cycles, the capacity

Table 6
Kinetic models employed in this work.

Model name	Equation	Fractional equation
Pseudo-First Order (PFO)	$q_t = q_e(1-\exp(-k_1 \cdot t))$	$\theta = 1-\exp(-k_1 \cdot t)$
Pseudo-Second Order (PSO)	$q_t = \frac{k_2 \cdot q_e^2 \cdot t}{1+k_2 \cdot q_e \cdot t}$	$\theta = \frac{k_2 \cdot q_e \cdot t}{1+k_2 \cdot q_e \cdot t}$
Modified Ritchie	$q_t = q_e(1-\frac{1}{\beta+k_m \cdot t})$	$\theta = 1-\frac{1}{\beta+k_m \cdot t}$
Avrami	$q_t = q_e(1-\exp(1-(k_A t)^{n_A}))$	$\theta = 1-\exp(1-(k_A t)^{n_A})$
Elovich	$q_t = \frac{1}{\beta}\ln(\alpha \cdot \beta)+\frac{1}{\beta}\ln(t)$	$\theta = \frac{1}{q_e}(\frac{1}{\beta}\ln(\alpha \cdot \beta)+\frac{1}{\beta}\ln(t))$
Intraparticle Diffusion	$q_t = c + k_d \cdot t^{0.5}$	$\theta = \frac{1}{q_e}(c + k_d \cdot t^{0.5})$

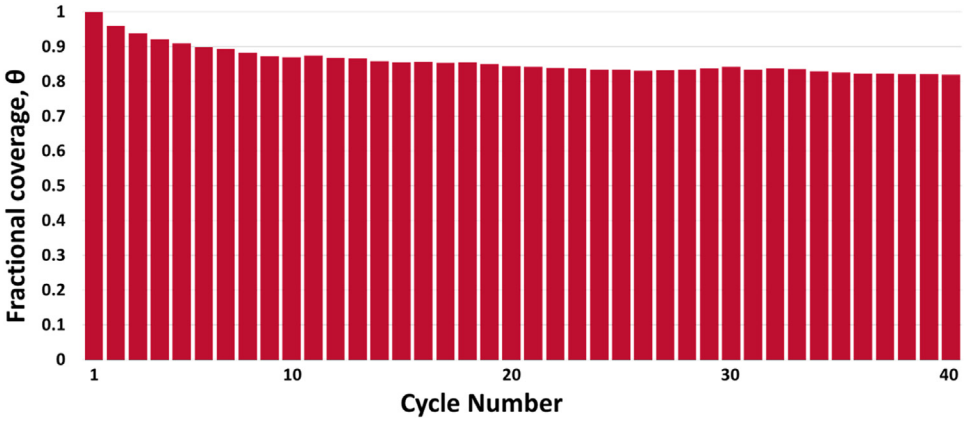

Fig. 7. Cyclic adsorption tests.

is 90 % of the original value (followed by 87 % after 20 cycles) until levelling at 85 % coverage between cycles 30 and 40.

ChAB shows a slightly more modest working capacity after 10 cycles than the physically activated AC derived from biomass combustion bottom ash (Gorbounov et al., 2023) though outperforms other alternative adsorbents, e.g. tetraethylenepentamine functionalized SBA-15 (Sanz-Pérez et al., 2013). Another amine-modified mesoporous silica (albeit in a pressure swing adsorption set-up) was shown to lose 4 % of capacity over 5 cycles (Dao et al., 2020), which is on par with ChAB.

The decreasing level of working capacity of the material developed in our work can be associated with the not full (i.e. partial) desorption from cycle to cycle. This phenomenon may have led to blockage of some pores as well as supressed capillary condensation upon desorption.

3.7.4. Heat of adsorption

Isosteric heat of adsorption (Q_{st}) is a paramount parameter for evaluating materials, especially in the context of temperature swing adsorption processes. Generally, it is calculated based on the volumetric gas adsorption measurements by utilising the Clausius–Clapeyron equation (Eq. (2)).

$$Q_{st} = -R\left[\partial \ln p / \partial\left(\frac{1}{T}\right)\right]_{q_e} \tag{2}$$

where R is the universal gas constant, p_i is the pressure at which an appropriate (same) adsorption capacity (q_e) is reached, whilst T_i is the temperature at which the isotherm measurements have been conducted. Common practice in the literature suggests employing four/five isotherms each spread no more than 10 – 15 °C apart. Alternatively, a minimum of two isotherm measurements within 20 °C from each other (or Δ10 °C for three) can also be used (Nuhnen and Janiak, 2020). Following this method, the isosteric heat of adsorption (pure CO_2) for ChAB has been calculated to be ~30.5 kJ/mol. As such, ChAB presents a heat of adsorption that is comparable to other similar physisorbents for CO_2 and lower than that of chemisorbents. For example, for KOH-activated carbonaceous adsorbents (derived from rice husk) the isosteric heats of adsorption were calculated to be in the range of ~25 – ~26.5 kJ/mol (Nandi et al., 2023). However, experimental values were not gathered for this particular adsorbent. With regards to measured heats of adsorption, experiments (adsorption of pure CO_2 at 40 °C) conducted on a number of amine-functionalised silicas proposed their Q_{st} values to vary in the range of 68 – 104 kJ/mol (Dao et al., 2020). Measurements for zeolites 13X and 5A show Q_{st} to be 47.6 and 53 kJ/mol, respectively (Gutierrez-Ortega et al., 2022). However, the latter values were obtained using a 15 % CO_2 + 85 % N_2 (v/v) mixture at 50 °C. An alternative measurement method (employing Helium as the purge and balance gas across different partial pressures of CO_2) showed the values for zeolite 13X to plateau at ~36.5 kJ/mol at 25 °C, whilst at 50 °C Q_{st} stabilised at approximately 38 – 39 kJ/mol (Son et al., 2018). The

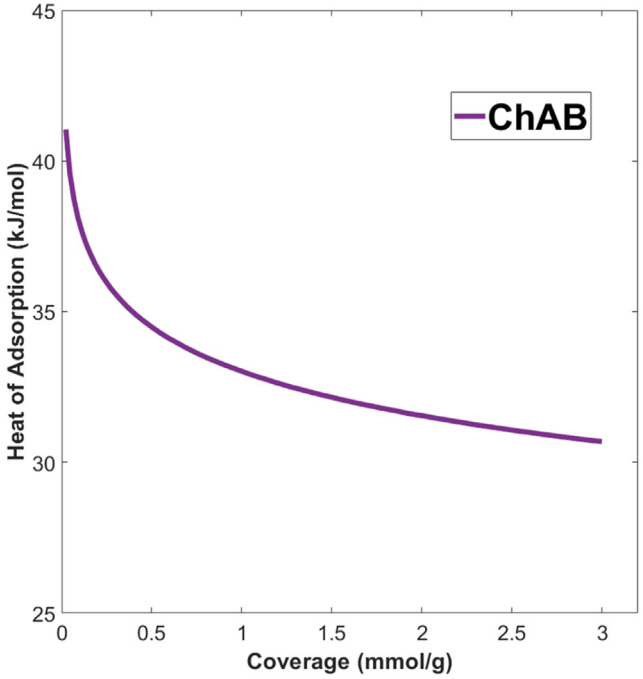

Fig. 8. ChAB heat of adsorption data.

latter results corroborate the hypothesis of the heat of adsorption being temperature dependant (Nuhnen and Janiak, 2020).

However, within the classical adsorption temperature range, a stronger dependence on adsorbate loading (rather than the temperature) is commonly observed (as can be visualised from Fig. 8). This occurs due to the high-energy (thermodynamically favoured) sites being occupied preferentially/first. As such, in the initial seconds a sharp increase in the enthalpy of adsorption can be observed which levels off once a plateau is reached (Son et al., 2018). The former phenomenon is associated with adsorption at zero coverage and the heat of adsorption at this stage often differs significantly from the data for the energy released (since adsorption is an exothermic process) from the "bulk" adsorption (Nuhnen and Janiak, 2020). In the cases of adsorption at high temperatures (less thermodynamically favourable conditions), the low energy sites (also less thermodynamically favourable) would not be occupied at all or to a lesser degree. Therefore, the adsorption process would not reach the "bulk" adsorption conditions, hence, preventing a strong decline in material's heat of adsorption.

Nevertheless, Q_{st} is of paramount value for industrial deployment of sorbent. This is due to the isosteric enthalpy of *adsorption* being the reverse of the enthalpy of *desorption* (Nuhnen and Janiak, 2020). As such,

minimising this parameter would lead to a lesser energy requirement for regeneration. Additionally, suboptimal heat of adsorption has been shown to prevent sorbents being highly selective as well as preclude them from having a high cyclic capacity (Wilmer et al., 2012).

Finally, since the absolute value of Q_{st} for ChAB is higher than the enthalpy of condensation of CO_2 (−17 kJ/mol), the sample is believed not to have reached full pore filling at the evaluated conditions (Nuhnen and Janiak, 2020).

4. Conclusion

Biomass combustion bottom ash-derived carbon has been chemically activated with KOH utilising a Taguchi DoE array to investigate the impact of different parameters onto the CO_2 adsorption capacity of the produced material. The findings suggest KOH to be an appropriate activating agent for CO_2 capture as a high degree of microporosity was observed on the surface of the carbon. Within that, moderate activation times (30 min) and temperatures (~625 °C) at relatively high ramp rates (10 – 15 °C/min) are suggested to be most favourable and impactful, whilst the impregnation ratio was found not to be statistically significant. The latter phenomenon could be attributed to the inherent heterogeneity of dry mixing (as opposed to wet mixing of activating agent and carbon). Additionally, the uncontrollable variation of waste matter also may have impacted the system. Nevertheless, following this approach, an adsorbent with a CO_2 uptake of 1.93 mmol/g and 1.29 mmol/g at 1 bar and 25 °C and 50 °C, respectively; cyclic stability of 85 % (following 40 adsorption-desorption cycles) and heat of adsorption of ~ 30.5 kJ/mol was produced and characterised.

Such approach to biomass combustion ash valorisation would facilitate (if implemented) waste management as well as constitute monetary savings for Drax (and/or any other biomass combusting facility). The problems associated with landfilling of any waste are well-known and addressing them by producing capture media for CO_2 (to be implemented *in-situ*) would help address two environmental issues simultaneously.

Further research may consider focusing on further purification of the precursor to minimise ash impurities as well as further characterisation of the adsorbent surface (e.g. X-ray photoelectron spectroscopy (XPS) and Boehm titration). Additionally, issues of adsorbent's selectivity (over both N_2 and moisture) as well as scale-up (in terms of the appropriate adsorbent particle shape (e.g. bead, pellet, tablet) and its size) can be investigated. This would allow to move forward towards breakthrough studies, hence, solving the questions of application within a particular adsorption reactor configuration (e.g. fixed or fluidised bed) utilising a particular regeneration regime (e.g. temperature or pressure swing adsorption) under conditions that would mimic those of a given post-combustion carbon capture system. These are imperative for generation of accurate and sophisticated process models which could then be deployed for techno-economic analysis purposes.

Data availability statement

Data have been made available in Brunel University London's repository *via* Brunel Figshare database.

Declaration of Competing Interest

The authors declare that they have no known competing financial interests or personal relationships that could have appeared to influence the work reported in this paper.

Acknowledgements

This work has been funded by the UK Carbon Capture and Storage Research Centre (EP/W002841/1) through the flexible funded research programme "Investigation of Environmental and Operational Challenges of Adsorbents Synthesised from Industrial Grade Biomass Combustion Residues". The UKCCSRC is supported by the Engineering and Physical Sciences Research Council (EPSRC), UK, as part of the UKRI Energy Programme.

Dr David Danaci would like to acknowledge funding provided by UK Research and Innovation (UKRI) under grants EP/P026214/1 and EP/T033940/1. Dr Salman Masoudi Soltani also acknowledges EPSRC for the financial support of this work (grant EP/T033940/1).

The authors would like to thank and acknowledge the undergraduate research assistants from the Department of Chemical Engineering at Brunel University London, Anila Islami and Jodie Baker for all their assistance during this project.

The authors would like to recognise the Experimental Techniques Centre (ETC) at Brunel University London and their scientific officers for facilitating access to analytical equipment.

The authors are grateful to Prof Paul S. Fennell (Imperial College London, UK) for facilitating the volumetric CO_2 isotherm measurements.

Last but not least, we would also like to acknowledge the continued generous support from Drax Group UK, with a special thanks to Dr James Hammerton throughout this research.

Supplementary materials

The volumetric CO_2 isotherm data has been provided as Supplementary Information in AIF format.

Supplementary material associated with this article can be found, in the online version, at doi:10.1016/j.ccst.2023.100151.

References

Assad Munawar, M., et al., 2021. Biomass ash characterization, fusion analysis and its application in catalytic decomposition of methane. Fuel 285 (July 2020), 119107. doi:10.1016/j.fuel.2020.119107.

ASTM, 2013. ASTM D3172-13, Standard Practice For Proximate Analysis of Coal and Coke Available at:. https://www.astm.org/Standards/D3172.htm.

Bade, M.M., et al., 2022. Highly efficient multisubstrate agricultural waste-derived activated carbon for enhanced CO 2 capture. ACS Omega 7 (22), 18770–18779. doi:10.1021/acsomega.2c01528.

Bai, J., Huang, J., Yu, Q., Demir, M., Akgul, E., et al., 2023a. Fabrication of coconut shell-derived porous carbons for CO2 adsorption application. Front. Chem. Sci. Eng. 17 (8), 1122–1130. doi:10.1007/s11705-022-2292-6.

Bai, J., Huang, J., Yu, Q., Demir, M., Kilic, M., et al., 2023b. N-doped porous carbon derived from macadamia nut shell for CO2 adsorption. Fuel Process. Technol. 249, 107854. doi:10.1016/j.fuproc.2023.107854.

Bansal, R.C., Goyal, M., 2005. *Activated Carbon adsorption, Activated Carbon Adsorption*. Taylor & Francis Group, CRC Press doi:10.1680/bwtse.63341.147.

BBC, 2022. The "Green" Row over the UK's Largest Renewable Power Plant 14 January. Available at:. https://www.bbc.co.uk/news/business-59546281 Accessed: 26 June 2023.

BEIS, 2021. Net Zero Strategy: Build Back Greener. Gov.Uk Available at. https://www.gov.uk/government/publications/net-zero-strategy .

Bottani, E.J., Tascón, J.M.D., 2008. Adsorption By Carbons.

Brunauer, S., Emmett, P.H., Teller, E., 1938. Adsorption of gases in multimolecular layers. J. Am. Chem. Soc. 60 (2), 309–319. doi:10.1021/ja01269a023.

Calzaferri, G., Gallagher, S.H., Brühwiler, D, 2022. Multiple equilibria describe the complete adsorption isotherms of nonporous, microporous, and mesoporous adsorbents. Microporous Mesoporous Mater. 330, 111563. doi:10.1016/j.micromeso.2021.111563.

Dao, D.S., Yamada, H., Yogo, K., 2020. Enhancement of CO2 adsorption/desorption properties of solid sorbents using tetraethylenepentamine/diethanolamine blends. ACS Omega 5 (37), 23533–23541. doi:10.1021/acsomega.0c01515.

Derrick, M.R., Stulik, D., Landry, J.M., 1999. *Infrared Spectroscopy in Conservation Science, Pract Surf Anal by Auger and X-ray Photoelectron Spectrosc*.

Drax, 2019. Drax sets world-first ambition to become carbon negative by 2030 Available at:. https://www.drax.com/press_release/drax-sets-world-first-ambition-to-become-carbon-negative-by-2030 . (Accessed: 26 June 2023).

Dubinin, M.M., 1975. Physical adsorption of gases and vapors in micropores. In: Progress in Surface and Membrane Science. Academic Press, Inc., pp. 1–70. doi:10.1016/B978-0-12-571809-7.50006-1.

Evans, J.D., et al., 2021. A universal standard archive file for adsorption data. Langmuir 37 (14), 4222–4226. doi:10.1021/acs.langmuir.1c00122.

Gorbounov, M., et al., 2021. Application of nanoporous carbon, extracted from biomass combustion ash, in CO 2 adsorption. In: 2021 IEEE 21st International Conference on Nanotechnology (NANO). IEEE, pp. 229–232. doi:10.1109/NANO51122.2021.9514288.

Gorbounov, M., Petrovic, B., et al., 2022. Development of nanoporosity on a biomass combustion ash-derived carbon for CO2 adsorption. In: 2022 IEEE

22nd International Conference on Nanotechnology (NANO). IEEE, pp. 245–248. doi:10.1109/NANO54668.2022.9928660.
Gorbounov, M., Taylor, J., et al., 2022. To DoE or not to DoE? A technical review on & roadmap for optimisation of carbonaceous adsorbents and adsorption processes. S. Afr. J. Chem. Eng. 41 (July), 111–128. doi:10.1016/j.sajce.2022.06.001.
Gorbounov, M., Petrovic, B., et al., 2023. Activated carbon derived from Biomass combustion bottom ash as solid sorbent for CO2 adsorption. Chem. Eng. Res. Des. 194, 325–343. doi:10.1016/j.cherd.2023.04.057.
Gorbounov, M., Diaz-Vasseur, E., et al., 2023. Impact of production pathway on nanoporosity of carbonaceous sorbents for CO 2 adsorption. In: 2023 IEEE 23rd International Conference on Nanotechnology (NANO). IEEE, pp. 249–254. doi:10.1109/NANO58406.2023.10231299.
Gutierrez-Ortega, A., et al., 2022. A fast methodology to rank adsorbents for CO2 capture with temperature swing adsorption. Chem. Eng. J. 435, 134703. doi:10.1016/j.cej.2022.134703.
Hattori, Y., Kaneko, K., Ohba, T., 2013. Adsorption properties. Compreh. Inorg. Chem. II 25–44. doi:10.1016/B978-0-08-097774-4.00502-7.
Heidarinejad, Z., et al., 2020. Methods for preparation and activation of activated carbon: a review. Environ. Chem. Lett. 18 (2), 393–415. doi:10.1007/s10311-019-00955-0.
Hossain, A., Ngo, H.H., Guo, W., 2013. Introductory of microsoft excel solver function - spreadsheet method for isotherm and kinetics modelling of metals biosorption in water and wastewater. J. Water Sustain. 3 (4), 223–237. Available at: http://www.jwsponline.com/uploadpic/Magazine/pp223-237JWS-A-13-013.pdf.
Huang, G., et al., 2019. Activated carbons prepared by the KOH activation of a hydrochar from garlic peel and their CO2 adsorption performance. New Carbon Mater. 34 (3), 247–257. doi:10.1016/S1872-5805(19)60014-4.
Ji, Y., et al., 2022. A high adsorption capacity bamboo biochar for CO2 capture for low temperature heat utilization. Sep. Purif. Technol. 293, 121131. doi:10.1016/j.seppur.2022.121131.
Kaloni, T.P., et al., 2012. K-intercalated carbon systems: effects of dimensionality and substrate. EPL (Europhys. Lett.) 98 (6), 67003. doi:10.1209/0295-5075/98/67003.
Karimi, M., et al., 2023. MIL-160(Al) as a candidate for biogas upgrading and CO2 capture by adsorption processes. Ind. Eng. Chem. Res. 62 (12), 5216–5229. doi:10.1021/acs.iecr.2c04150.
Ketabchi, M.R., et al., 2023. Latest advances and challenges in carbon capture using bio-based sorbents: a state-of-the-art review. Carbon Capture Sci. Technol. 6 (October 2022), 100087. doi:10.1016/j.ccst.2022.100087.
Kiełbasa, K., et al., 2022. Carbon dioxide adsorption over activated carbons produced from molasses using H2SO4, H3PO4, HCl, NaOH, and KOH as activating agents. Molecules 27 (21), 7467. doi:10.3390/molecules27217467.
Konopka, J., 2013. *Options for quantitative analysis of light elements by SEM/EDS, Thermo Fisher Scientific Technical Note 52523* Available at:. https://assets.thermofisher.com/TFS-Assets/CAD/Warranties/TN52523_E_0713M_LightElement_H.pdf.
Lemmon, E.W., et al., 2023. *Thermophysical Properties of Fluid Systems, NIST Chemistry WebBook, NIST Standard Reference Database Number 69*. National Institute of Standards and Technology, Gaithersburg, MD Edited by P. J. Linstrom and W. G. Mallard20899 doi:10.18434/T4D303.
Liu, J., et al., 2015. Spherical potassium intercalated activated carbon beads for pulverised fuel CO2 post-combustion capture. Carbon N. Y. 94, 243–255. doi:10.1016/j.carbon.2015.06.036.
Ma, C., et al., 2022. Water chestnut shell-derived N/S-doped porous carbons and their applications in CO2 adsorption and supercapacitor. Fuel 326, 125119. doi:10.1016/j.fuel.2022.125119.
Map: Organic Chemistry (Wade), Infrared Spectra of Some Common Functional Groups, 2020. LibreTexts Available at:. https://chem.libretexts.org/@go/page/45261.
Masoudi Soltani, S., et al., 2015. Lead removal from aqueous solution using non-modified and nitric acid-modified charred carbon from the pyrolysis of used cigarette filters. Desalination Water Treat. 53 (1), 126–138. doi:10.1080/19443994.2013.835751.
McClellan, A., Harnsberger, H., 1967. Cross-sectional areas of molecules adsorbed on solid surfaces. J. Colloid Interface Sci. 23 (4), 577–599. doi:10.1016/0021-9797(67)90204-4.
Merck, 2023. IR Spectrum Table & Chart Available at. https://www.sigmaaldrich.com/GB/en/technical-documents/technical-article/analytical-chemistry/photometry-and-reflectometry/ir-spectrum-table . Accessed: 13 June 2023.
Michalik, M., Wilczynska-Michalik, W., 2012. Mineral and chemical composition of biomass ash. Eur. Mineral. Conf. 1 (July 2014), 2012–2423. doi:10.13140/2.1.4298.5603.
Molina-Sabio, M., Rodríguez-Reinoso, F., 2004. Role of chemical activation in the development of carbon porosity. Colloids Surf. A: Physicochem. Eng. Aspects 241 (1–3), 15–25. doi:10.1016/j.colsurfa.2004.04.007.
Mozaffari Majd, M., et al., 2022. Adsorption isotherm models: a comprehensive and systematic review (2010–2020). Sci. Total Environ. 812 (xxxx). doi:10.1016/j.scitotenv.2021.151334.
Nandi, R., et al., 2023. Impact of KOH activation on rice husk derived porous activated carbon for carbon capture at flue gas alike temperatures with high CO2/N2 Selectivity. ACS Omega 8 (5), 4802–4812. doi:10.1021/acsomega.2c06955.
Nuhnen, A., Janiak, C., 2020. A practical guide to calculate the isosteric heat/enthalpy of adsorption via adsorption isotherms in metal–organic frameworks, MOFs'. Dalton Trans. 49 (30), 10295–10307. doi:10.1039/D0DT01784A.
Office for National Statistics, 2023. 2021 UK Greenhouse Gas Emissions Available at:. https://assets.publishing.service.gov.uk/government/uploads/system/uploads/attachment_data/file/1134664/greenhouse-gas-emissions-statistical-release-2021.pdf.
Oladoja, N.A., 2016. A critical review of the applicability of Avrami fractional kinetic equation in adsorption-based water treatment studies. Desalination Water Treat. 57 (34), 15813–15825. doi:10.1080/19443994.2015.1076355.
Patel, H.A., Byun, J., Yavuz, C.T., 2017. Carbon dioxide capture adsorbents: chemistry and methods. ChemSusChem 10 (7), 1303–1317. doi:10.1002/cssc.201601545.
Petrovic, B., et al., 2021. Biomass combustion fly ash-derived nanoporous zeolites for post-combustion carbon capture. In: 2021 IEEE 21st International Conference on Nanotechnology (NANO). IEEE, pp. 233–236. doi:10.1109/NANO51122.2021.9514342.
Petrovic, B., et al., 2022a. Synthesis of nanoporous type A and X zeolite mixtures from biomass combustion fly ash for post-combustion carbon capture. In: 2022 IEEE 22nd International Conference on Nanotechnology (NANO). IEEE, pp. 221–224. doi:10.1109/NANO54668.2022.9928679.
Petrovic, B., Gorbounov, M., Masoudi Soltani, S., 2022b. Impact of surface functional groups and their introduction methods on the mechanisms of CO2 adsorption on porous carbonaceous adsorbents. Carbon Capture Sci. Technol. 3, 100045. doi:10.1016/j.ccst.2022.100045.
Quan, C., et al., 2023. Biomass-based carbon materials for CO2 capture: a review. J. CO2 Util. 68, 102373. doi:10.1016/j.jcou.2022.102373.
Quan, C., Su, R., Gao, N., 2020. Preparation of activated biomass carbon from pine sawdust for supercapacitor and CO 2 capture. Int. J. Energy Res. 44 (6), 4335–4351. doi:10.1002/er.5206.
Rashidi, N.A., Yusup, S., 2021. Co-valorization of delayed petroleum coke – palm kernel shell for activated carbon production. J. Hazard. Mater. 403, 123876. doi:10.1016/j.jhazmat.2020.123876.
Rouquerol, J. et al. (2013) *Adsorption by Powders and Porous Solids: principles, Methodology and Applications: second Edition, Adsorption by Powders and Porous Solids: principles, Methodology and Applications: second Edition*. doi:10.1016/C2010-0-66232-8.
Sajjadi, B., et al., 2019. Chemical activation of biochar for energy and environmental applications: a comprehensive review. Rev. Chem. Eng. 777–815. doi:10.1515/revce-2018-0003.
Sanz-Pérez, E.S., et al., 2013. CO2 adsorption performance of amino-functionalized SBA-15 under post-combustion conditions. Int. J. Greenh. Gas Control 17, 366–375. doi:10.1016/j.ijggc.2013.05.011.
Shafeeyan, M.S., et al., 2010. A review on surface modification of activated carbon for carbon dioxide adsorption. J. Anal. Appl. Pyrolysis 89 (2), 143–151. doi:10.1016/j.jaap.2010.07.006.
Simonin, J.P., 2016. On the comparison of pseudo-first order and pseudo-second order rate laws in the modeling of adsorption kinetics. Chem. Eng. J. 300, 254–263. doi:10.1016/j.cej.2016.04.079.
Sinha, P., et al., 2019. Surface area determination of porous materials using the Brunauer–Emmett–Teller (BET) method: limitations and Improvements. J. Phys. Chem. C 123 (33), 20195–20209. doi:10.1021/acs.jpcc.9b02116.
Sivarajasekar, N., Baskar, R., 2019. Adsorption of Basic Magenta II onto H2SO4 activated immature Gossypium hirsutum seeds: kinetics, isotherms, mass transfer, thermodynamics and process design. Arab. J. Chem. 12 (7), 1322–1337. doi:10.1016/j.arabjc.2014.10.040.
Son, K.N., et al., 2018. Measurement and prediction of the heat of adsorption and equilibrium concentration of CO2 on zeolite 13X. J. Chem. Eng. Data 63 (5), 1663–1674. doi:10.1021/acs.jced.8b00019.
Songolzadeh, M., Soleimani, M., Takht Ravanchi, M., 2015. Using modified Avrami kinetic and two component isotherm equation for modeling of CO2/N2 adsorption over a 13X zeolite bed. J. Nat. Gas Sci. Eng. 27, 831–841. doi:10.1016/j.jngse.2015.09.029.
Taylor, J.H., Masoudi Soltani, S., 2023. Carbonaceous adsorbents in the removal of aquaculture pollutants: a technical review of methods and mechanisms. Ecotoxicol. Environ. Saf. 266, 115552. doi:10.1016/j.ecoenv.2023.115552.
Terrones, G.G., et al., 2023. SESAMI APP: an accessible interface for surface area calculation of materials from adsorption isotherms. J. Open Source Softw. 8 (86), 5429. doi:10.21105/joss.05429.
Thommes, M., et al., 2015. Physisorption of gases, with special reference to the evaluation of surface area and pore size distribution (IUPAC Technical Report). Pure Appl. Chem. 87 (9–10), 1051–1069. doi:10.1515/pac-2014-1117.
UK Biomass Policy Statement, 2021. Department for Business Energy & Industrial Strategy, p. 45 Available at:.
Vassilev, S.V., et al., 2010. An overview of the chemical composition of biomass. Fuel 89 (5), 913–933. doi:10.1016/j.fuel.2009.10.022.
Wang, S., et al., 2022. Development of high-performance adsorbent using KOH-impregnated rice husk-based activated carbon for indoor CO2 adsorption. Chem. Eng. J. 437, 135378. doi:10.1016/j.cej.2022.135378.
Williams, N.E., Oba, O.A., Aydinlik, N.P., 2022. Modification, production, and methods of KOH-activated carbon. ChemBioEng Rev. 9 (2), 164–189. doi:10.1002/cben.202100030.
Wilmer, C.E., et al., 2012. Structure-property relationships of porous materials for carbon dioxide separation and capture. Energy Environ. Sci. 5 (12), 9849–9856. doi:10.1039/c2ee23201d.
Woszuk, A., Bandura, L., Franus, W., 2019. Fly ash as low cost and environmentally friendly filler and its effect on the properties of mix asphalt. J. Clean. Prod. 235, 493–502. doi:10.1016/j.jclepro.2019.06.353.
Yun, C.M. et al. (2022) 'Bottom and fly ash as sand and portland cement filler replacement in high volume concrete', in, pp. 121–132. doi:10.1007/978-3-030-98812-8_7.
Zhai, J., Burke, I.T., Stewart, D.I., 2021. Beneficial management of biomass combustion ashes. Renew. Sustain. Energy Rev. 151, 111555. doi:10.1016/j.rser.2021.111555.
Zhang, J., et al., 2022. Carboxylic functionalized mesoporous polymers for fast, highly efficient, selective and reversible adsorption of ammonia. Chem. Eng. J. 448, 137640. doi:10.1016/j.cej.2022.137640.